Synthesis, Characterization and Comparative Gas Sensing Study of ZnO–GO and ZnO–rGO Compounds

N.S. Hosseini[a], J. Hasanzadeh[a,*] and A. Abdolahzadeh Ziabari[b]

[a] *Department of Physics, Faculty of Science, Takestan Branch, Islamic Azad University, Takestan, Iran*
[b] *Nano Research Lab, Lahijan Branch, Islamic Azad University, Lahijan, Iran*

Received: 11.01.2022 & Accepted: 08.03.2022

Doi: 10.12693/APhysPolA.141.591 *e-mail: javadhasanzadeh649@gmail.com

In this work, we prepare composites of ZnO–GO and ZnO–rGO through an economic and facile route and comparatively study their gas sensitivity towards ethanol. The morphological, compositional, and structural properties of the prepared composites are investigated using scanning electron microscopy, energy-dispersive X-ray spectroscopy, and X-ray diffraction analysis. The optimal work temperature of 300°C was observed for the prepared samples. The ZnO–GO-based sensor shows higher sensitivity than ZnO–rGO. Also, the variation of response and recovery time with the gas concentration is investigated. As expected, the sensitivity increases as the gas concentration increases. In addition, it was revealed that the response and recovery time is a function of the surface morphology.

topics: gas sensor, graphene, ZnO, sensitivity

1. Introduction

Gas sensors are employed for the detection of toxic, diffuse, and combustible gases. These devices are also extensively utilized in industry and firefighting. Various types of materials have been studied to fabricate gas sensors, such as optical fibers [1], inorganic semiconductors [2], polymers [3], and carbon nanomaterials [4]. Graphene has been attracting a lot of attention as a gas sensing material since 2004, when it was discovered. It shows a high specific area (2630 m^2/g), high mobility (20 000 cm^2/V s) at room temperature, the highest surface-to-volume ratio among the known layered materials, and low electrical noise [5]. One of the graphene compounds, graphene oxide (GO), is an electrical insulator mainly due to pendent oxygen functional groups that restrict it for gas sensing. The conductivity of GO can be restored close to graphene by the elimination of oxygen functional groups and the restoration of aromatic double bonded carbons through chemical reduction or high temperature heat treatment [6, 7]. The process of reduction has a remarkable effect on how close reduced graphene oxide (rGO) is achieved, in terms of structure, to porous graphene (PG) and its quality. Compared to PG, in the detection of different gases, rGO has shown more promising properties in terms of low production cost, fine tuning structure, dispersibility to water, feasibility of further modification, premium electrical conductivity, and chemically active defect sites [6]. Many efforts have been carried out to increase the gas sensing of rGO, such as hybridization with metal oxides and polymers and functionalization with different chemical groups [8, 9]. Recently, hybrid structures of rGO and metal oxide semiconductor (MOS) structures have been investigated for highly sensitive, selective, and economical gas sensors that work at low temperatures [5]. Nanostructured MOSs, such as ZnO, SnO_2, and Cu_2O, are widely used in gas sensing devices due to their high specific surface area, large aspect ratio, and good flexibility. However, these nanostructures have poor electrical conductivity. The hybridization of MOSs with two-dimensional graphene can effectively improve their electrical conductivity and sensing performance. ZnO is extensively used and has a wide range of applications, including gas sensors, transparent electrodes, optoelectronic devices, etc. [10]. ZnO-based gas sensors usually work at a temperature range of 200–450°C [11]. Working at high temperature increases the redox reactions underlying the sensing mechanism of chemiresitors. Hence, the reduction of a working temperature is crucial in the fabrication of chemical sensors with low power consumption and small size. In this study, we report the synthesis and characterization of nanoparticle composites of ZnO–rGO and ZnO–GO through a facile and low-cost method. The aim is to perform a comparative study of the gas sensing capability of the produced composites, which is scarce in the literature. The sensing traits of the achieved compounds have been analyzed toward ethanol gas at different work temperatures and gas concentrations.

2. Experimental details

Initially, 1 mg of graphene oxide was dissolved in 15 ml of isopropanol using an ultrasonic bath for 1.5 h. Then, to prepare the ZnO solution, 2.6 g of zinc acetate was dissolved in 30 ml of ethanol and stirred at 70°C for 2 h. During the stirring, diethanolamine was added as the stabilizer to the solution until a transparent solution was obtained. Then the yielded solution containing the graphene oxide was centrifuged for 4 min at 4000 rpm. After centrifugation, the sediment phase was removed and the left homogenous solution was kept for the next step. A solution of graphene oxide with a volume of 10 ml was then mixed with 20 ml of zinc acetate solution and the obtained mixture was placed in an ultrasonic bath for 1 h. This solution was then used for the preparation of thin films by the dip-coating method. Before dip-coating, the soda lime substrates were initially degreased with detergent and washed thoroughly with deionized water. Next, to remove the macroscopic contaminations, the substrates were cleaned ultrasonically in a surfactant containing ethanol and acetone (each of 50% in volume). The cleaned substrates were dipped into the prepared solution, and withdrawn from it vertically at a speed of 116 mm/min. The coated glass substrate was then dried at 150°C for 10 min in an oven to evaporate the solvent and organic residuals. This procedure was repeated 20 times. Then the dried thin films were post annealed in air at 450°C for 1 h, and the powder samples were prepared from the solution used for thin film deposition. The exact same procedure was used to prepare a composition of reduced graphene oxide and zinc oxide. Finally, two types of compounds containing ZnO–GO and ZnO–rGO, both in the form of thin films, were prepared.

3. Characterization

The structure of the prepared thin films was studied by the X-ray diffraction (XRD) method using a PANalytical X'PERT PRO with Cu K_α radiation ($\lambda = 0.15406$ nm). The surface morphology of the films was studied by field effect scanning electron microscopy (FESEM) with a TESCAN MIRA3 instrument equipped with energy-dispersive X-ray spectroscopy (EDX) for surface chemical composition analysis. Gas sensing analysis of the samples toward ethanol injection was carried out using a homemade static system [12]. The response of the device for reducing gas is determined as [13]

$$S = \frac{R_a\,(\Omega)}{R_g\,(\Omega)} = \frac{\frac{V_C(V)}{V_{Ra}(V)} - 1}{\frac{V_C(V)}{V_{Rg}(V)} - 1}, \tag{1}$$

where R_a and R_g are the baseline resistance of the sensing film in pure air and in a gas environment, respectively. The quantities of V_{R_g} and V_{R_a} denote the voltages of variable resistor with and without ethanol ambient, respectively. The response time is the time taken for the sample resistance to reach 90% of the equilibrium value after injection of the test gas. The recovery time is defined as the required time for the sample to return to 10% of its original resistance in air after the removal of the test gas.

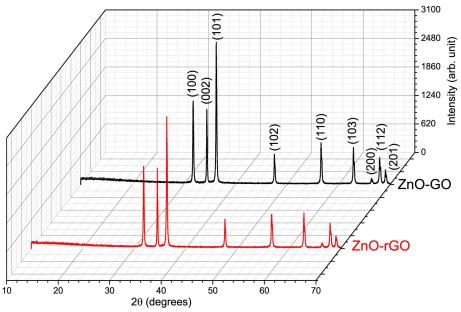

Fig. 1. XRD patterns of the grown ZnO–GO and ZnO–rGO thin films.

4. Results and discussion

The XRD pattern of the prepared ZnO–GO and ZnO–rGO thin films has been displayed in Fig. 1. The diffraction peaks show the reflections (100), (002), (101), (102), (110), (103), (200), (112), and (201) of ZnO in a hexagonal Wurtzite lattice which agrees with JCPDS No. 36-1451 of ZnO [14].

The lack of any secondary phase confirms the synthesis of single phase ZnO nanocrystals. The average crystallite size of the samples was evaluated by the Scherrer's equation [15]

$$D = \frac{0.9\lambda}{\beta\,\cos(\theta)}, \tag{2}$$

where β is the full width at half maximum (FWHM) of the peak (in radians), θ is the Bragg's diffraction angle at the peak position, and λ is the wavelength of the X-ray radiation.

The average crystallite size for ZnO–GO and ZnO–rGO nanocomposite was found to be 85 nm and 20 nm, respectively. As it is clearly seen in Fig. 1, no diffraction peak related to GO and rGO is observed. It can be due to (1) lesser amount of GO and rGO than ZnO, giving relatively low diffraction intensity in the synthesized nanocomposite, and (2) that fact that anchoring of ZnO nanoparticles on GO and rGO might hinder the restacking of carbon sheets, which leads to weak diffraction peak or no diffraction peak at all [16, 17].

The backscattered electron scanning electron microscope (BSE-SEM) images showing the morphology and EDX mappings of localized microstructure in ZnO–GO and –rGO thin films are shown in Fig. 2. It confirms that Zn, O, and C are the main elements in the samples. The results have been shown quantitively in Fig. 3 and Table I.

Figure 4 shows the scanning electron microscope (SEM) results of the films. To investigate the influence of GO and rGO on the nanoparticle distribution in the samples, FESEM analyses of ZnO–GO

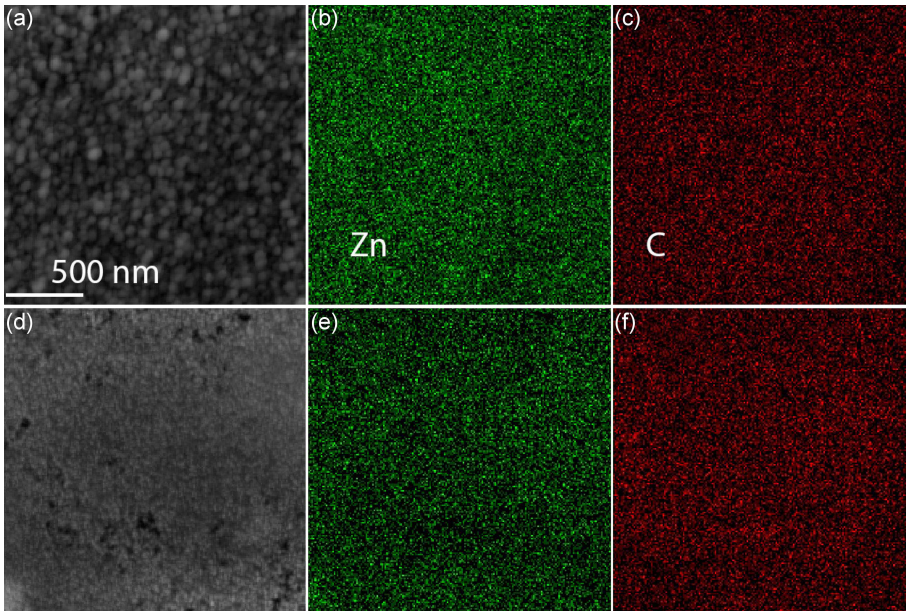

Fig. 2. EDX mapping of elemental composition of (a–c) ZnO–GO and (d–f) ZnO–rGO thin films.

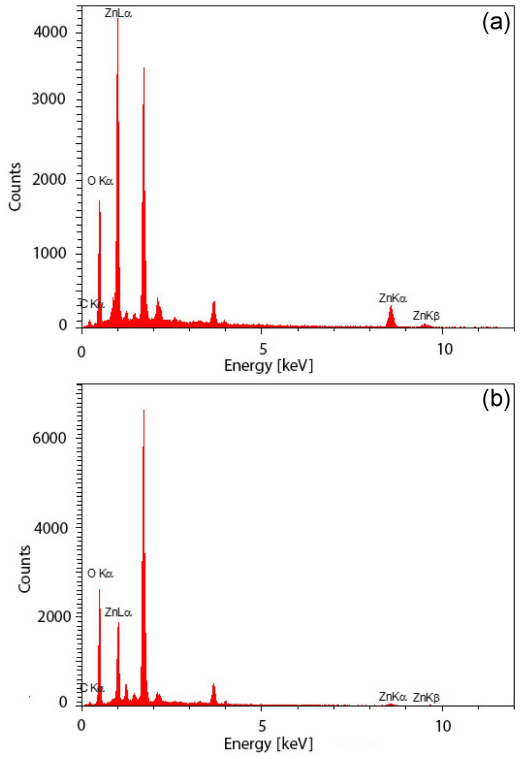

Fig. 3. The EDX spectra of (a) ZnO–GO and (b) ZnO–rGO thin films.

and ZnO–rGO were performed. The microstructure of ZnO–GO and ZnO–rGO thin films at different magnifications is shown in Fig. 4. The FESEM images clearly show the hexagonal agglomeration of ZnO–GO nanoparticles with an average size of 90 nm and the spherical ZnO–rGO nanoparticles with an average size of 20 nm. As observed in Fig. 4,

TABLE I

Quantitative analysis of structure based on ZnO–GO and ZnO–rGO.

Element	Line	Int.	Error	Wt%	At.%
ZnO–GO					
C	K_α	9.2	20.36	5.71	12.24
O	K_α	347.3	21.04	41.67	67.04
Zn	K_α	154.4	0.53	52.62	20.72
ZnO–rGO					
C	K_α	9.5	11.97	6.27	9.14
O	K_α	496.6	12.37	79.58	87.07
Zn	K_α	20.9	0.51	14.15	3.79

the presence of rGO significantly affects the size distribution and morphology of the nanoparticles. Finer nanoparticles distributed on a less porous morphology are obviously seen. A more careful and closer view reveals that the individual ZnO–rGO nanoparticles with the size of 20 nm are well separated from each other and well distributed on the surface.

The gas sensitivity of the prepared thin films was analyzed by exposing the samples to ethanol vapor. The variability in the resistance of the prepared thin films was monitored through the measurement of the voltage of a variable resistor. Through the adsorption and desorption of oxygen on the surface of the MOSs, the electrical resistance changes. The MOS thin film adsorbs the oxygen molecules as it is exposed to air. The adsorption increases as the temperature increases, and the adsorbed oxygen molecules oxidize the surface MOSs. Consequently, O^{2-} ions emerge, leading to an increase

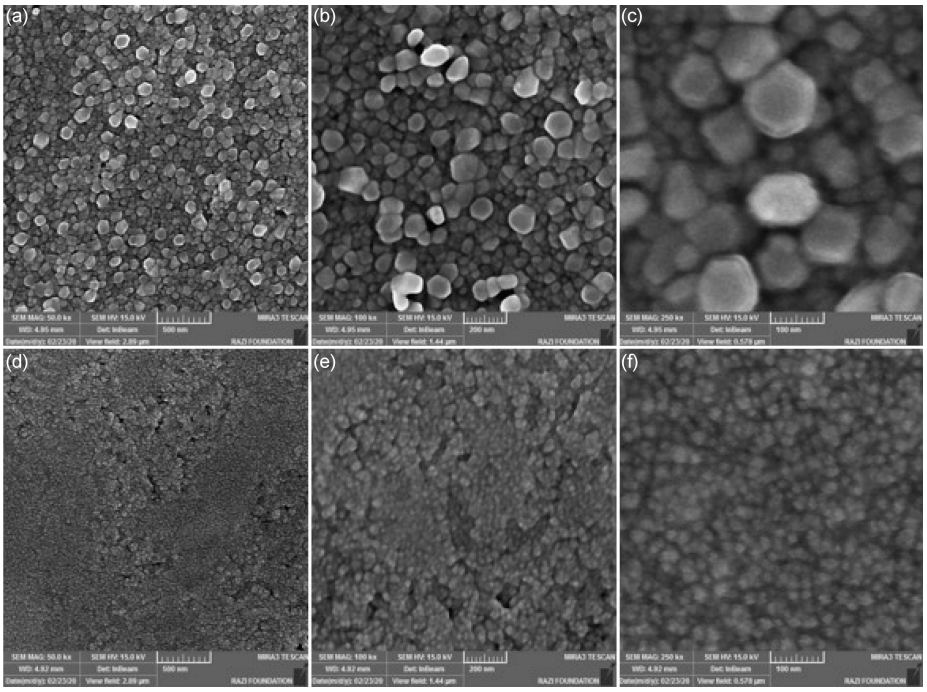

Fig. 4. FESEM images of (a–c) ZnO–GO samples and (d–f) ZnO–rGO samples. These SEM images at different magnifications changed from 500 to 100 nm.

in sensor resistance. When ethanol is introduced, a reaction between oxygen ions and the adsorbed ethanol molecules occurs, which releases electrons back to the conduction band, followed by a decrease in the sensor resistance. Because almost all MOS gas sensors have no good response at room temperature, finding an optimal operating temperature is the main problem. Fortunately, the synergistic effects of ZnO doped with graphene drastically improve the sensitivity of ZnO gas sensors [18]. It is believed that the combination of ZnO with functionalized graphene is a promising remedy for the problems of the development of ZnO-based gas sensors with low working temperatures and high sensitivity [19]. We followed this solution to improve the performance of the prepared ZnO gas sensors.

The sensitivity of the thin films under injection of 1200 ppm ethanol is displayed in Fig. 5. As can be observed, the working temperature for both samples is the same at 300°C. Compared to the reported values for pure ZnO thin film prepared by the same method and conditions [20], it seems very promising. According to [20], the highest sensitivity for the pure ZnO was attained around 400°C, with an ethanol concentration of 2500 ppm.

In Fig. 5, when not at the optimal temperature, the sensitivity decreases drastically. This trend is commonly linked to the gas adsorption/desorption events on the surface of the sensor. When the working temperature is low, the thermal energy is not sufficient to overcome the activation energy barrier, and no reaction with the absorbed oxygen occurs. When the temperature increases,

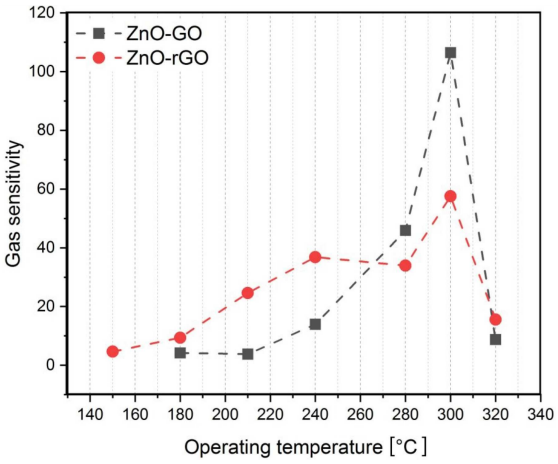

Fig. 5. Gas sensitivity of the samples at different operating temperatures for ZnO–GO and ZnO–rGO thin films (ethanol concentration 1200 ppm).

sufficient O^{2-} molecules present themselves on the surface to react with ethanol vapor molecules. Accordingly, an improvement in sensor performance is observed. At temperatures higher than optimal, the performance is deteriorated mainly due to a smaller amount of adsorbed O^{2-} compared to the desorbed O^{2-}, as well as evaporation of ethanol molecules before reaction.

The time of the response (T_{res}) and recovery (T_{rec}) are key factors in determining the performance of the gas sensor. The time when the resistance reaches stability after the injection of the gas

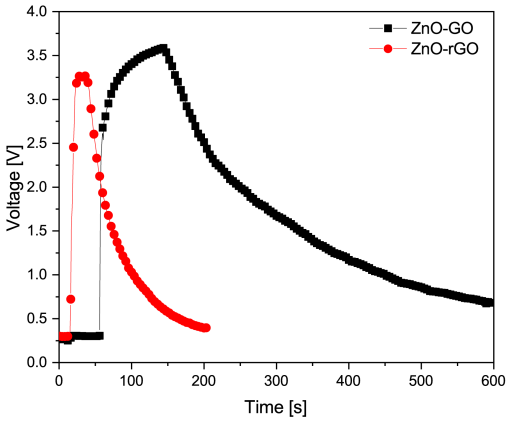

Fig. 6. The real-time dynamic response of ZnO–GO and ZnO–rGO thin films upon exposure to 1200 ppm of ethanol at 300°C.

is illustrated by T_{res}, while T_{rec} is the time when the resistance reaches 90% of the initial value in the air. The real-time dynamic response curve of ZnO–GO and ZnO–rGO to 1200 ppm ethanol gas at 13 V is depicted in Fig. 6. One can see that T_{res} = 64 s and the T_{rec} = 120 s for ZnO–GO, and T_{res} = 13 s and T_{rec} = 35 s for ZnO–rGO. The reason for the observed difference between the response time of ZnO–GO and ZnO–rGO can be assigned mainly to the lower speed of the adsorption and desorption of ethanol, and more porosity of ZnO–GO thin films, which operate as reaction centers compelling oxygen and ethanol molecules to stay long enough to perform the gas-sensing reaction.

The performance of a gas sensor is a function of the gas concentration. When the gas concentration is low, the probability of interaction decreases. At higher gas concentrations, more gas molecules interact with the chemisorbed oxygen molecules, leading to a more intense response. The real-time dynamic response of ZnO–GO and ZnO–rGO thin films upon exposure to different concentrations of ethanol at 300°C has been shown in Fig. 7. As illustrated in Fig. 7a and b, the curve rises as the ethanol vapor is injected into the test system and declines rapidly when the ethanol vapor is released. The response amplitude of the thin films gradually grows when the gas concentration increases from 600 to 1680 ppm. The response and recovery properties of ZnO–GO and ZnO–rGO thin films are approximately reproducible, which implies the stability of the response of the prepared thin films. Those are critical features for the commercial application of any electronic device. The calculated sensitivity of the samples as a function of the gas concentration is shown in Fig. 7c. It is clear that the sensitivity of both ZnO–GO and ZnO–rGO thin films increases with the ethanol vapor concentration. Also, the sensing characteristics related to ZnO–GO thin film seem more appropriate than those of ZnO–rGO in the detection of ethanol.

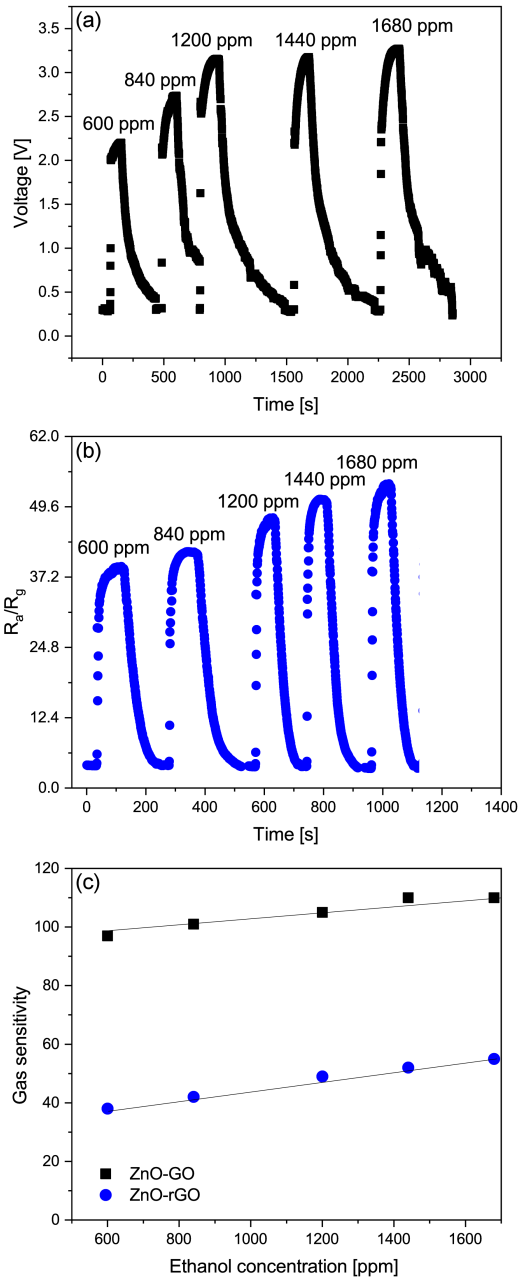

Fig. 7. Response of (a) ZnO–GO and (b) ZnO–rGO based sensor and (c) the related sensitivity in different ethanol vapor concentrations.

5. Conclusions

In summary, ZnO–GO and ZnO–rGO thin films were successfully grown by a facile and economical method. The pertinent structural, morphological, compositional, and gas sensing properties of the films were studied in detail. The structural measurement showed a wurtzite hexagonal structure related to polycrystalline ZnO. The morphological features of the samples revealed evenly distributed nanograins on the surface of the films. The compositional measurement confirmed the presence of Zn, O, and C in the compounds. The samples showed

an appropriate sensitivity towards ethanol gas. Especially the working temperature of the ZnO-based gas sensor improved as ZnO was alloyed with GO and rGO. We achieved the promising work temperature of 300°C for the synthesized thin films. The dynamic response and recovery characteristics of the films were studied comparatively. Results show that the prepared ZnO–GO thin film can be a very good candidate for ethanol gas sensors.

Acknowledgments

All authors would like to thank Dr. Abbas Bagheri Khatibani for his helpful advice on various technical issues examined in this paper.

References

[1] W.H. Chua, M.H. Yaacob, C.Y. Tan, B.H. Ong, *Ceram. Int.* **47**, 32828 (2021).

[2] A. Bagheri Khatibani, A. Abdolahzadeh Ziabari, S.M. Rozati, Z. Bargbidi, G. Kiriakidis, *Trans. Electr. Electron. Mater.* **13**, 111 (2012).

[3] M. Hao, R. Zhang, X. Jia, X. Gao, W. Gao, L. Cheng, Y. Qin, *Sens. Actuator A Phys.* **332**, 113173 (2021).

[4] S. Nejatinia, S.K. Charvadeh, A. Bagheri Khatibani, *Jpn. J. Appl. Phys.* **61**, 017001 (2022).

[5] N.B. Thakare, F.C. Raghuwanshi, V.S. Kalyamwar, Y.S. Tamgadge, *AIP Conf. Proc.* **1953**, (2018) 030057.

[6] F. Yavari, N. Koratkar, *J. Phys. Chem. Lett.* **3**, 1746 (2012).

[7] A. Lipatov, A. Varezhnikov, P. Wilson, V. Seysoev, A. Kolmakov, A. Sinitskii, *Nanoscale* **5**, 5426 (2013).

[8] F.-L. Meng, Z. Guo, X.-J. Huang, *Trends Analyt. Chem.* **68**, 37 (2015).

[9] W. Yuan, G. Shi, *J. Mater. Chem. A* **1**, 10078 (2013).

[10] K. Ahmadi, A. Abdolahzadeh Ziabari, K. Mirabbaszadeh, A. Ahadpour Shal, *Bull. Mater. Sci.* **38**, 617 (2015).

[11] M.J.S. Spencer, *Prog. Mater. Sci.* **57**, 437 (2012).

[12] A. Bagheri Khatibani, M. Abbasi, *J. Sol–Gel Sci. Technol.* **86**, 255 (2018).

[13] A. Bagheri Khatibani, *J. Electron. Mater.* **48**, 3784 (2019).

[14] Joint Committee on Powder Diffraction, Powder Diffraction File, Card 36-1451 (ZnO), ICDD, Swarthmore (PA) 1996.

[15] A. Abdolahzadeh Ziabari, N.M. Zindanlou, J. Hassanzadeh, S. Golshahi, A.B. Khatibani, *J. Alloy Compd.* **842**, 155741 (2020).

[16] C. Xu, X. Wang, J. Zhu, *J. Phys. Chem. C* **112**, 19841 (2008).

[17] X. Liu, L. Pan, Q. Zhao, T. Lv, G. Zhu, T. Chen, T. Lu, Z. Sun, C. Sun, *Chem. Eng. J.* **183**, 238 (2012).

[18] G. Lu, S. Park, K. Yu, R.S. Ruoff, L.E. Ocola, D. Rosenmann, J. Chen, *ACS Nano* **5**, 1154 (2011).

[19] J. Li, W. Zhang, J. Sun, *Ceram. Int.* **42**, 9851 (2016).

[20] A. B. Khatibani, *Indian J. Phys.* **95**, 243 (2021).